

## Accepted Manuscript

Molecular structure, FT-IR, FT-Raman, NBO, HOMO and LUMO, MEP, NLO and molecular docking study of 2-[(*E*)-2-(2-bromophenyl)ethenyl]quinoline-6-carboxylic acid

Rajeev T. Ulahannan, C. Yohannan Panicker, Hema Tresa Varghese, Robert Musiol, Josef Jampilek, Christian Van Alsenoy, Javeed Ahmad War, S.K. Srivastava

PII: S1386-1425(15)30014-7  
DOI: <http://dx.doi.org/10.1016/j.saa.2015.06.077>  
Reference: SAA 13847

To appear in: *Spectrochimica Acta Part A: Molecular and Biomolecular Spectroscopy*

Received Date: 10 November 2014  
Revised Date: 20 June 2015  
Accepted Date: 22 June 2015

Please cite this article as: R.T. Ulahannan, C. Yohannan Panicker, H.T. Varghese, R. Musiol, J. Jampilek, C. Van Alsenoy, J.A. War, S.K. Srivastava, Molecular structure, FT-IR, FT-Raman, NBO, HOMO and LUMO, MEP, NLO and molecular docking study of 2-[(*E*)-2-(2-bromophenyl)ethenyl]quinoline-6-carboxylic acid, *Spectrochimica Acta Part A: Molecular and Biomolecular Spectroscopy* (2015), doi: <http://dx.doi.org/10.1016/j.saa.2015.06.077>

This is a PDF file of an unedited manuscript that has been accepted for publication. As a service to our customers we are providing this early version of the manuscript. The manuscript will undergo copyediting, typesetting, and review of the resulting proof before it is published in its final form. Please note that during the production process errors may be discovered which could affect the content, and all legal disclaimers that apply to the journal pertain.



Molecular structure, FT-IR, FT-Raman, NBO, HOMO and LUMO, MEP, NLO and molecular docking study of 2-[(*E*)-2-(2-bromophenyl)ethenyl]quinoline-6-carboxylic acid Rajeev T.Ulahannan<sup>a</sup>, C.Yohannan Panicker<sup>a\*</sup>, Hema Tresa Varghese<sup>b</sup>, Robert Musiol<sup>c</sup>, Josef Jampilek<sup>d</sup>, Christian Van Alsenoy<sup>e</sup>, Javeed Ahmad War<sup>f</sup>, S.K.Srivastava<sup>f</sup>

<sup>a</sup>Department of Physics, TKM College of Arts and Science, Kollam, Kerala, India.

<sup>b</sup>Department of Physics, Fatima Mata National College, Kollam, Kerala, India.

<sup>c</sup>Institute of Chemistry, University of Silesia, Szkolna 9, 40007 Katowice, Poland.

<sup>d</sup>Department of Chemical Drugs, Faculty of Pharmacy, University of Veterinary and Pharmaceutical Sciences Brno, Palackeho 1/3, 61242 Brno, Czech Republic.

<sup>e</sup>University of Antwerp, Chemistry Department, Universiteitsplein 1, B2610 Antwerp, Belgium.

<sup>f</sup>Department of Chemistry, Dr.H.S.Gour Central University, Sagar, M.P. 470003, India.

\*author for correspondence: email: [cyphyp@rediffmail.com](mailto:cyphyp@rediffmail.com)

Phone: 91 9895370968

### Abstract

The optimized molecular structure, vibrational frequencies, corresponding vibrational assignments of 2-[(*E*)-2-(2-bromophenyl)ethenyl]quinoline-6-carboxylic acid have been investigated experimentally and theoretically using Gaussian09 software package. Potential energy distribution of the normal modes of vibrations was done using GAR2PED program. <sup>1</sup>H-NMR chemical shifts calculations were carried out by using B3LYP functional with SDD basis set. The HOMO and LUMO analysis is used to determine the charge transfer within the molecule. The stability of the molecule arising from hyper-conjugative interaction and charge delocalization has been analyzed using NBO analysis. MEP was performed by the DFT method and the predicted infrared intensities and Raman activities have also been reported. The calculated geometrical parameters are in agreement with that of similar derivatives. The title compound forms a stable complex with PknB as is evident from the binding affinity values and the molecular docking results suggest that the compound might exhibit inhibitory activity against PknB and this may result in development of new anti-tuberculosic agents.

**Keywords:** DFT; FT-IR; FT-Raman; quinoline; MEP; Molecular docking.

### 1. Introduction

Quinoline derivatives fascinate much interest due to their anti-amoebic, antiviral [1, 2], anti-parasitic [3], antimicrobial [4] and anti-tubercular activities [5]. They possess anti-proliferative [6], anti-neoplastic [7], and cytotoxic properties [8]. Quinolines have been detected in meteorite extracts, and in general quinolines are of astrobiological interest, since this class of molecule includes nucleobases, basic components of nucleic acids [9, 10]. Quinoline derivatives could be used as dopants in the polymer-LED materials [11]. They could generate a sharp green electroluminescence and have high quantum efficiency of emission in the blue and the green region [12, 13]. Quinoline based dyes have developed with the advent of technology and are applied to electroluminescence and photochromism as well as the field of medication [14, 15]. Quinoline possesses non-centro symmetry and hence they are used in the synthesis of molecules having non-linear optical responses [16, 17]. They are widely used in electrochemical sensing [18] and optical switching devices [19]. In the present work, IR and Raman spectra of the title compound are reported both experimentally and theoretically. NBO, molecular electrostatic potential, NMR studies, first and second hyperpolarizability are also reported. Due to the different potential biological activity of the title compound, molecular docking of the title compound is also reported.

### 2. Experimental details

2-Methylquinoline-6-carboxylic acid was obtained by the Skraup synthesis from 4-aminobenzoic acid and crotonaldehyde. To a refluxing solution of 1.0 equiv of 4-aminobenzoic acid, was added dropwise over three hour period 1.2 equiv of crotonaldehyde.

The resulting mixture was heated under reflux for 2 hour. After being cooled aqueous ammonia was added to pH 3 and the mixture was extracted with  $\text{CH}_2\text{Cl}_2$ . The organic layer was washed with brine, dried over magnesium sulfate and concentrated under vacuum. The crude product was recrystallized from ethanol. This quinolinecarboxylic acid (10 mmol) was thoroughly mixed with 2-bromobenzaldehyde (20 mmol) and exposed to microwave irradiation for 6 min. After the reaction was completed the crude product was washed with diethyl ether (15 ml). Recrystallization from ethanol yielded the target 2-[(*E*)-2-(2-bromophenyl)ethenyl]quinoline-6-carboxylic acid [20, 21]. Scheme 1 is provided as supporting material.

The FT-IR spectrum (Fig. 1) was recorded using KBr pellets on a DR/Jasco FT-IR 6300 spectrometer. The spectral resolution was  $4\text{cm}^{-1}$ . The FT-Raman spectrum (Fig. 2) was obtained on a Bruker RFS 100/s, Germany. For excitation of the spectrum the emission of Nd:YAG laser was used with excitation wavelength 1064 nm and maximal power 150 mW; measurement were performed on solid samples. One thousand scans were accumulated with a total registration time of about 30 min. The spectral resolution after apodization was  $2\text{cm}^{-1}$ . Raman spectrum in the ranges  $1750\text{-}3250\text{cm}^{-1}$  and  $250\text{-}1550\text{cm}^{-1}$  are provided as supporting material Fig.S1 and Fig.S2.  $^1\text{H-NMR}$  spectra was recorded on a Bruker AM-500 (500 MHz for  $^1\text{H}$ ), Bruker BioSpin Corp., Germany. Chemical shifts are reported in ppm ( $\delta$ ) to internal  $\text{Si}(\text{CH}_3)_4$ , when diffused easily exchangeable signals are omitted.

### 3. Computational details

Calculations of the title compound are carried out with Gaussian09 program [22] using the B3PW91/6-31G(6D,7F), B3LYP/6-31G(6D,7F) and B3LYP/SDD quantum chemical calculation methods to predict the molecular structure and vibrational wave numbers. Molecular geometry was fully optimized by Berny's optimization algorithm using redundant internal coordinates. Harmonic vibrational wave numbers are calculated using the analytic second derivatives to confirm the convergence to minima on the potential energy surface. The DFT hybrid B3LYP functional and SDD methods tend to overestimate the fundamental modes, therefore scaling factor of 0.9613 has to be used for all the theoretically obtained wavenumbers for obtaining a considerably better agreement with experimental data [23]. The Stuttgart/Dresden effective core potential basis set (SDD) was chosen particularly because of its advantage of doing faster calculations with relatively better accuracy and structures [24, 25]. Then frequency calculations were employed to confirm the structure as minimum points in energy. Parameters corresponding to optimized geometry (SDD) of the title compound (Fig. 3) are given in Table 1. The absence of imaginary wavenumbers on the calculated vibrational spectrum confirms that the structure deduced corresponds to minimum energy. The assignments of the calculated wave numbers are aided by the animation option of GAUSSVIEW program, which gives a visual presentation of the vibrational modes [26]. The potential energy distribution (PED) is calculated with the help of GAR2PED software package [27].

## 4. Results and Discussion

### 4.1. IR and Raman spectra

The calculated wavenumbers (scaled), observed IR and Raman bands and assignments are given in Table 2. In the following discussion, experimental values are compared with B3LYP/SDD values, since these values are in agreement with the experimental data. The carboxylic group is characterized by the OH stretch, C=O stretch and OH out-of-plane deformation and by the C-O stretch and OH in-plane deformation. For the title compound, the OH stretching is assigned at  $3522\text{cm}^{-1}$  theoretically. The C=O stretching vibration in the spectra of carboxylic acids give rise to a strong band in the region  $1600\text{-}1700\text{cm}^{-1}$  [28]. The band observed at  $1634\text{cm}^{-1}$  in Raman and  $1627\text{cm}^{-1}$  in SDD is assigned as C=O stretching mode. The OH in-plane deformation, coupled to C-O stretching mode is

expected in the region  $1390 \pm 55 \text{ cm}^{-1}$  [28], and the band at  $1323 \text{ cm}^{-1}$  in IR,  $1314 \text{ cm}^{-1}$  in Raman and  $1308 \text{ cm}^{-1}$  in SDD is assigned as the in-plane bending of OH group which is not pure but contains contributions from other modes also. The C(=O)O stretching mode coupled to OH in-plane bending exhibits a band in the region  $1250 \pm 80 \text{ cm}^{-1}$  and the band at  $1272 \text{ cm}^{-1}$  in SDD is assigned as this mode. The deformation modes, out-of-plane OH, in-plane C=O and out of plane C=O are expected in the region  $905 \pm 65, 725 \pm 95$  and  $595 \pm 85 \text{ cm}^{-1}$  respectively [29]. These bands are assigned at  $900 \text{ cm}^{-1}$  (SDD),  $708$  (IR) and  $723$  (SDD),  $518$  (SDD) respectively. Ulahannan et al. [30] reported the  $\gamma\text{OH}$  mode at  $926$  and  $\delta\text{C=O}$  at  $766 \text{ cm}^{-1}$ .

Benzene ring possesses six ring-stretching vibrations, of which the four with the highest wavenumbers (occurring near  $1600, 1580, 1490$  and  $1440 \text{ cm}^{-1}$ ) are good group vibrations. With heavy substituent, the bands tend to shift to somewhat lower wavenumbers. In the absence of ring conjugation, the band at  $1580 \text{ cm}^{-1}$  is usually weaker than that at  $1600 \text{ cm}^{-1}$ . The fifth ring-stretching vibration is active near  $1315 \pm 65 \text{ cm}^{-1}$ , a region that overlaps strongly with that of the CH in-plane deformation. The sixth ring-stretching vibration, or the ring-breathing mode, appears as a weak band near  $1000 \text{ cm}^{-1}$  in mono-, 1,3-di- and 1,3,5-trisubstituted benzenes. In the otherwise substituted benzenes, however, this vibration is substituent sensitive and difficult to distinguish from the ring in plane deformation [28]. For the tri-substituted benzene ring PhI, the ring stretching modes are observed at  $1476, 1392, 1236 \text{ cm}^{-1}$  in IR,  $1593, 1500, 1385, 1239 \text{ cm}^{-1}$  in Raman and  $1600, 1527, 1474, 1383, 1234 \text{ cm}^{-1}$  in SDD. This is in agreement with the expected values [28]. In the asymmetric tri-substituted benzenes, when all the three substituent are light, the frequency interval of the ring breathing mode is between  $500$  and  $600 \text{ cm}^{-1}$ . When all the three substituent are heavy, the frequency appears above  $1100 \text{ cm}^{-1}$ . In the case of mixed substituent the frequency is expected to appear between  $600$  and  $750 \text{ cm}^{-1}$  [28]. For the title compound the PhI ring breathing mode is observed at  $738 \text{ cm}^{-1}$  in SDD. Mary et al. [31] reported the mode at  $733 \text{ cm}^{-1}$  in IR and  $738 \text{ cm}^{-1}$  theoretically.

For the ortho substituted benzene the PhII stretching modes are expected in the range  $1620\text{-}1260 \text{ cm}^{-1}$  [28] and in the present case, these modes at  $1588, 1534, 1421, 1296 \text{ cm}^{-1}$  in IR,  $1463, 1396 \text{ cm}^{-1}$  in Raman and  $1574, 1537, 1453, 1402, 1300 \text{ cm}^{-1}$  in SDD. In ortho di-substitution, the ring-breathing mode has three wavenumber intervals according to whether both substituents are heavy, or one of them is heavy while the other is light, or both of them are light. In the first case, the interval is  $1100\text{-}1130 \text{ cm}^{-1}$ , in the second case it is  $1020\text{-}1070 \text{ cm}^{-1}$ , while in the third case [32] it is  $630\text{-}780 \text{ cm}^{-1}$ . In the present case, the band observed at  $1098 \text{ cm}^{-1}$  in IR and  $1104 \text{ cm}^{-1}$  in SDD is assigned as the ring breathing mode.

The C-H stretching occurs above  $3000 \text{ cm}^{-1}$  for benzene ring [33]. In the present case the bands at  $3130, 3106, 3091 \text{ cm}^{-1}$  in SDD for 1,2,4 tri-substituted benzene and  $3118, 3103, 3087, 3071 \text{ cm}^{-1}$  for 1,2-di-substituted benzene are assigned as the C-H stretching modes. The in-plane CH vibrations are expected in the range of  $1010\text{-}1300 \text{ cm}^{-1}$ ,  $1290\text{-}1050 \text{ cm}^{-1}$  for ortho substituted benzenes [28] and 1,2,4 tri-substituted benzenes, respectively. The modes at  $1123 \text{ cm}^{-1}$  in IR,  $1117 \text{ cm}^{-1}$  in Raman and  $1259, 1146, 1123 \text{ cm}^{-1}$  in SDD are assigned as  $\delta\text{CH}$  mode for 1,2,4 tri-substituted benzene. Also the modes at  $1154, 1098, 1023 \text{ cm}^{-1}$  in IR,  $1158, 1023 \text{ cm}^{-1}$  in Raman and  $1272, 1160, 1104, 1031 \text{ cm}^{-1}$  in SDD are assigned as  $\delta\text{CH}$  mode for ortho substituted benzene. The C-H out-of-plane deformations are observed between  $1000$  and  $700 \text{ cm}^{-1}$  [28]. The out-of-plane CH vibrations are determined by the number of adjacent hydrogen atoms on the ring. 1,2,4-trisubstituted benzenes show a medium absorption in the range  $940\text{-}840 \text{ cm}^{-1}$  and a strong band in the range  $940\text{-}840 \text{ cm}^{-1}$ .

For the title compound we observed these modes at  $852 \text{ cm}^{-1}$  in IR,  $929 \text{ cm}^{-1}$  in Raman and  $990, 930, 852 \text{ cm}^{-1}$  in SDD. The bands at  $960, 745 \text{ cm}^{-1}$  in IR,  $965 \text{ cm}^{-1}$  in Raman and  $993, 960, 868, 740 \text{ cm}^{-1}$  in SDD are assigned as this mode. The CH stretching

modes outside the benzene rings are assigned at 3057  $\text{cm}^{-1}$  in IR, 3045  $\text{cm}^{-1}$  in Raman and 3147, 3115, 3079 3044  $\text{cm}^{-1}$  in SDD. In the present case C=C and C-C stretching modes are assigned at 1616, 1196  $\text{cm}^{-1}$  (IR), 1618  $\text{cm}^{-1}$  (Raman) and 1623, 1184  $\text{cm}^{-1}$  (SDD).

The CBr stretching vibrations are expected in the range 635 $\pm$ 85  $\text{cm}^{-1}$  [28, 34]. The band at 638  $\text{cm}^{-1}$  in IR and 635  $\text{cm}^{-1}$  in SDD is assigned as this mode. Varghese et al. [35] reported this mode at 637  $\text{cm}^{-1}$  (IR), 639  $\text{cm}^{-1}$  (Raman) and 632  $\text{cm}^{-1}$  (SDD). Varghese et al. [35] reported the in-plane and out of plane bending of CBr at 207  $\text{cm}^{-1}$  and 120  $\text{cm}^{-1}$  respectively, where we assigned these modes at 227  $\text{cm}^{-1}$  (Raman), 254  $\text{cm}^{-1}$  (SDD) and 158  $\text{cm}^{-1}$  (SDD) respectively.

For the quinoline ring, the stretching modes are assigned at 1563  $\text{cm}^{-1}$  in IR spectrum, 1560  $\text{cm}^{-1}$  in Raman spectrum and 1568  $\text{cm}^{-1}$  theoretically (C=C stretching mode), 1500  $\text{cm}^{-1}$  in Raman spectrum and 1527  $\text{cm}^{-1}$  theoretically (C=N stretching mode), 1281  $\text{cm}^{-1}$  in IR spectrum, 1285  $\text{cm}^{-1}$  in Raman spectrum and 1285  $\text{cm}^{-1}$  theoretically (C-N stretching mode), 1476  $\text{cm}^{-1}$  in IR, 1205  $\text{cm}^{-1}$  in Raman, 1204 and 1474  $\text{cm}^{-1}$  theoretically (C-C stretching modes). The in-plane bending of the ring is assigned at 942, 813, 622  $\text{cm}^{-1}$  in IR and 946, 803, 802, 621, 522  $\text{cm}^{-1}$  in SDD. The other deformation modes of the phenyl and quinoline rings are identified and assigned in the Table 2. Chowdhury et al. [36] reported the ring vibrations of quinoline ring at 1245, 1383, 1434, 1470, 1593, 1621  $\text{cm}^{-1}$  in the Raman spectra and 760  $\text{cm}^{-1}$  as the ring breathing mode; the in-plane bending was reported by them at 526, 472, 508, 624, 829, 869  $\text{cm}^{-1}$ .

In order to investigate the performance of vibrational wavenumbers of the title compound, root mean square (RMS) values of wavenumbers were calculated using the

expression,  $\text{RMS} = \sqrt{\left(\frac{1}{n-1}\right) \sum_i^n (v_i^{\text{calc}} - v_i^{\text{exp}})^2}$ . The RMS error of the observed IR bands and Raman bands were found to be 12.47 (B3PW91/6-31G(6D, 7F)), 10.65 (B3LYP/6-31G(6D, 7F)), 8.62 (B3LYP/SDD) and 13.78 (B3PW91/6-31G(6D, 7F)), 11.85 (B3LYP/6-31G(6D, 7F)), 10.45 (B3LYP/SDD), respectively. The small difference between experimental and calculated vibrational modes may be due to the fact that experimental results belong to the solid phase and theoretical calculations belong to gaseous phase.

#### 4.2. Optimised geometrical parameters

To best of our knowledge, no X-ray crystallographic data of the title compound have yet been reported. However, the theoretical results (SDD) obtained are almost comparable with the reported structural parameters of similar derivatives. For the title compound the bond length of C<sub>1</sub>-C<sub>6</sub> is 0.0428 Å less than that of C<sub>1</sub>-C<sub>2</sub> (1.4290 Å) because of the delocalisation of electrons due to the presence of C(=O)OH group. The bond length of C<sub>4</sub>-C<sub>5</sub> (1.3958 Å) is also less than that of C<sub>3</sub>-C<sub>4</sub> (1.4197 Å) owing to the delocalisation of electrons. The bond length of C<sub>2</sub>-C<sub>3</sub> is 1.4418 Å. This large value for the bond length is due to the delocalisation of electron density due to the adjacent quinoline ring. The lesser bond length of C<sub>10</sub>=O<sub>11</sub> (1.2452 Å) could assigned due to the double bond character of that bond. The reported values of bond length for C<sub>1</sub>-C<sub>2</sub>, C<sub>1</sub>-C<sub>6</sub>, C<sub>2</sub>-C<sub>3</sub>, C<sub>4</sub>-C<sub>5</sub> and C<sub>10</sub>-O<sub>11</sub> are 1.4211, 1.3859, 1.4181, 1.4218 and 1.2311 Å [37]. For the title compound the bond length C<sub>26</sub>-C<sub>29</sub>, C<sub>26</sub>-Br<sub>34</sub>, C<sub>29</sub>-H<sub>32</sub> are 1.4057, 1.9693, 1.0853 Å respectively while the reported values are 1.37, 1.92, 1.0853 Å [38-40]. The bond angles C<sub>5</sub>-C<sub>10</sub>-O<sub>11</sub>, C<sub>5</sub>-C<sub>10</sub>-O<sub>12</sub>, O<sub>11</sub>-C<sub>10</sub>-O<sub>12</sub> and C<sub>10</sub>-O<sub>12</sub>-H<sub>13</sub> are 125.9, 112.9, 121.2 and 110.2° respectively which are in agreement with the reported values 124.1, 114.6, 121.3, 106.6° for the respective bond angles [39]. For the title compound the bond angles C<sub>2</sub>-N<sub>15</sub>-C<sub>19</sub>, C<sub>14</sub>-C<sub>17</sub>-H<sub>18</sub>, C<sub>14</sub>-C<sub>17</sub>-C<sub>19</sub>, N<sub>15</sub>-C<sub>19</sub>-C<sub>17</sub>, C<sub>24</sub>-C<sub>26</sub>-Br<sub>34</sub> and C<sub>29</sub>-C<sub>26</sub>-Br<sub>34</sub> are 119.4, 120.1, 119.8, 121.5, 123.7, 114.2° respectively. The reported values for these bond angles are 118.6, 120.9, 118.0, 123.6, 120.9 and 118.4° respectively [39-42].

#### 4.3. Frontier molecular orbitals

HOMO (Highest Occupied Molecular Orbital) and LUMO (Lowest Unoccupied Molecular Orbital) are the very important parameters for quantum chemistry. The eigen values of HOMO and LUMO and their energy gap reflect the biological activity of the molecule. A molecule having a small frontier orbital gap is more polarisable and is generally associated with a high chemical reactivity and low kinetic stability [43-45]. HOMO which can be thought as the outer orbital containing electrons tends to give these electrons as an electron donor and hence the ionization potential is directly related to the energy of the HOMO. On the other hand, LUMO can accept electrons and the LUMO energy is directly related to electron affinity (Fig. 4). Two important molecular orbital were examined for the title compound, HOMO and LUMO which are given in Fig. 4. The chemical potential, global hardness and electrophilicity will pave the way to understand the structure and reactivity of the molecule, with the aid of DFT based descriptors. Using HOMO and LUMO orbital energies, the ionization energy and electron affinity can be expressed as:  $I = -E_{\text{HOMO}}$ ,  $A = -E_{\text{LUMO}}$ ,  $\eta = (-E_{\text{HOMO}} + E_{\text{LUMO}})/2$  and  $\mu = (E_{\text{HOMO}} + E_{\text{LUMO}})/2$  [46]. Parr et al. [47] proposed the global electrophilicity power of a ligand as  $\omega = \mu^2/2\eta$ . This index measures the stabilization in energy when the system acquired an additional electronic charge from the environment. Electrophilicity encompasses both the ability of an electrophile to acquire additional electronic charge and the resistance of the system to exchange electronic charge with the environment. It contains information about both electron transfer (chemical potential) and stability (hardness) and is a better descriptor of global chemical reactivity. The hardness  $\eta$  and chemical potential  $\mu$  are given by the following relations:  $\eta = (I - A)/2$  and  $\mu = -(I+A)/2$ , where  $I$  and  $A$  are the first ionization potential and electron affinity of the chemical species [48]. For the title compound,  $E_{\text{HOMO}} = -8.57\text{eV}$ ,  $E_{\text{LUMO}} = -6.55\text{eV}$ , energy gap =  $E_{\text{LUMO}} - E_{\text{HOMO}} = 2.02\text{eV}$ , ionization potential  $I = 8.57\text{eV}$ , electron affinity  $A = 6.55\text{eV}$ , global hardness  $\eta = 1.01\text{eV}$ , chemical potential  $\mu = -7.56\text{eV}$  and global electrophilicity  $\omega = \mu^2/2\eta = 28.29\text{eV}$ . It is seen that the chemical potential of the title compound is negative and it means that the compound is stable. They do not decompose spontaneously into the elements they are made up of. The hardness signifies the resistance towards the deformation of electron cloud of chemical systems under small perturbation encountered during the chemical process. The principle of hardness works in chemistry and physics but it is not physically observable. Soft systems are large and highly polarisable, while hard systems are relatively small and much less polarisable.

#### 4.4. Molecular Electrostatic Potential

MEP is related to the electron density (ED) and is a very useful descriptor in understanding sites for electrophilic and nucleophilic reactions as well as hydrogen bonding interactions [49, 50]. The electrostatic potential  $V(r)$  is also well suited for analyzing processes based on the "recognition" of one molecule by another, as in drug-receptor, and enzyme-substrate interactions, because it is through their potentials that the two species first "see" each other [51,52]. To predict reactive sites of electrophilic and nucleophilic attacks for the investigated molecule, MEP at the B3LYP/SDD optimized geometry was calculated. The negative (red and yellow) regions of MEP were related to electrophilic reactivity and the positive (blue) regions to nucleophilic reactivity (Fig.S3-supporting material).

#### 4.5. Natural Bond Orbital Analysis

The Natural Bond Orbital (NBO) calculations were performed using NBO 3.1 program [53] as implemented in the Gaussian09 package at the B3LYP/SDD level in order to understand various second-order interactions between the filled orbital of one subsystem and vacant orbital of another subsystem, which is a measure of the inter-molecular delocalization or hyper-conjugation. NBO analysis provides the most accurate possible 'natural Lewis structure' picture of 'j' because all orbital details are mathematically chosen to include the highest possible percentage of the electron density. A useful aspect of the NBO method is

that it gives information about interactions of both filled and virtual orbital spaces that could enhance the analysis of intra and inter-molecular interactions. The second-order Fock-matrix was carried out to evaluate the donor-acceptor interactions in the NBO basis. The interactions result in a loss of occupancy from the localized NBO of the idealized Lewis structure into an empty non-Lewis orbital. For each donor (i) and acceptor (j) the stabilization energy (E2) associated with the delocalization  $i \rightarrow j$  is determined as:

$$E(2) = \Delta E_{ij} = q_i \frac{(F_{i,j})^2}{(E_j - E_i)}$$

where,  $q_i \rightarrow$  donor orbital occupancy,  $E_i, E_j \rightarrow$  diagonal elements and  $F_{ij} \rightarrow$  the off diagonal NBO Fock matrix element.

In NBO analysis large E(2) value shows the intensive interaction between electron-donors and electron-acceptors, and greater the extent of conjugation of the whole system, the possible intensive interaction are given in Table 3. The second-order perturbation theory analysis of Fock-matrix in NBO basis shows strong inter-molecular hyper-conjugative interactions are formed by orbital overlap between  $n(O)$ ,  $n(Br)$  and  $\sigma^*(C-O)$ ,  $\sigma^*(C-C)$  bond orbital which result in ICT causing stabilization of the system. These interactions are observed as an increase in electron density in C-O and C-C orbital that weakens the respective bonds. There occurs a strong inter-molecular hyper-conjugative interaction of  $C_{10}-O_{12}$  from  $O_{11}$  of  $n_2(O_{11}) \rightarrow \sigma^*(C_{10}-O_{12})$  which increases ED(0.11896e) that weakens the respective bonds  $C_{10}-O_{12}$  leading to stabilization of 32.30 kJ/mol and also the hyper-conjugative interaction of  $C_{10}-O_{12}$  from  $O_{12}$  of  $n_3(O_{12}) \rightarrow \sigma^*(C_{10}-O_{12})$  which increases ED (0.11896e) that weakens the respective bonds  $C_{10}-O_{12}$  leading to stabilization of 7.62 kJ/mol. Again a hyper-conjugative interaction of  $C_{24}-C_{26}$  from  $Br_{34}$  of  $n_3(Br_{34}) \rightarrow \sigma^*(C_{24}-C_{26})$  which increases ED (0.04050e) that weakens the respective bonds  $C_{24}-C_{26}$  leading to stabilization of 8.33 kJ/mol. These interactions are observed as an increase in electron density (ED) in C-C and C-O orbital that weakens the respective bonds. The increased electron density at the oxygen atoms leads to the elongation of respective bond length and a lowering of the corresponding stretching wave number. The electron density (ED) is transferred from the  $n(O)$  to the bonding  $\sigma^*$  orbital of the C-C and C-O bonds, explaining both the elongation and the red shift [54]. The hyper-conjugative interaction energy was deduced from the second-order perturbation approach. Delocalization of electron density between occupied Lewis-type (bond or lone pair) NBO orbital and formally unoccupied (anti bond or Rydberg) non-Lewis NBO orbital corresponds to a stabilizing donor-acceptor interaction. The COOH stretching modes can be used as a good probe for evaluating the bonding configuration around the atoms and the electronic distribution in the ring. Hence the title compound is stabilized by these orbital interactions. The NBO analysis also describes the bonding in terms of the natural hybrid orbital  $n_2(O_{11})$ , which occupy a higher energy orbital (-0.28112 a.u) with considerable p-character (100.00%) and low occupation number (1.86239) and the other  $n_1(O_{11})$  occupy a lower energy orbital(-0.70643a.u) with p-character (35.75%) and high occupation number (1.97615).The NBO analysis also describes the bonding in terms of the natural hybrid orbital  $n_2(O_{12})$ , which occupy a higher energy orbital (-0.34311 a.u) with considerable p-character (100.00%) and low occupation number (1.83339) and the other  $n_1(O_{12})$  occupy a lower energy orbital(-0.60506 a.u) with p-character (53.38%) and high occupation number (1.97983). The NBO analysis also describes the bonding in terms of the natural hybrid orbital  $n_3(Br_{34})$ , which occupy a higher energy orbital(-0.29284a.u) with considerable p-character (100.00%) and low occupation number (1.93812) and the other  $n_1(Br_{34})$  occupy a lower energy orbital(-0.69299 a.u) with p-character (12.04%) and high occupation number (1.99049).Thus, a very close to pure p-type lone pair orbital participates in the electron donation to the  $\sigma^*(C_{10}-O_{12})$  orbital for  $n_2(O_{11}) \rightarrow \sigma^*(C_{10}-O_{12})$ ,  $\sigma^*(C_{10}-O_{12})$

orbital for  $n_3(\text{O}_{12}) \rightarrow \sigma^*(\text{C}_{10}-\text{O}_{12})$ , and  $\sigma^*(\text{C}_{24}-\text{C}_{26})$  orbital for  $n_3(\text{Br}_{34}) \rightarrow \sigma^*(\text{C}_{24}-\text{C}_{26})$  interaction in the compound. The results are tabulated in Table S1 (supporting material).

#### 4.6. Nonlinear Optical Properties

Nonlinear optics deals with the interaction of applied electromagnetic fields in various materials to generate new electromagnetic fields, altered in wavenumber, phase, or other physical properties [55]. Organic molecules able to manipulate photonic signals efficiently are of importance in technologies such as optical communication, optical computing, and dynamic image processing [56, 57]. In this context, the dynamic first hyperpolarizability and average second hyperpolarizability of the title compound is also calculated in the present study. The first hyperpolarizability ( $\beta_0$ ) of this novel molecular system is calculated using SDD method, based on the finite field approach. In the presence of an applied electric field, the energy of a system is a function of the electric field. First hyperpolarizability is a third rank tensor that can be described by a  $3 \times 3 \times 3$  matrix. The 27 components of the 3D matrix can be reduced to 10 components due to the Kleinman symmetry [58]. The components of  $\beta$  are defined as the coefficients in the Taylor series expansion of the energy in the external electric field. When the electric field is weak and homogeneous, this expansion becomes

$$E = E_0 - \sum_i \mu_i F^i - \frac{1}{2} \sum_{ij} \alpha_{ij} F^i F^j - \frac{1}{6} \sum_{ijk} \beta_{ijk} F^i F^j F^k - \frac{1}{24} \sum_{ijkl} \gamma_{ijkl} F^i F^j F^k F^l + \dots$$

where  $E_0$  is the energy of the unperturbed molecule,  $F^i$  is the field at the origin,  $\mu_i$ ,  $\alpha_{ij}$ ,  $\beta_{ijk}$  and  $\gamma_{ijkl}$  are the components of dipole moment, polarizability, the first hyperpolarizability, and second hyperpolarizability, respectively. The calculated first hyperpolarizability of the title compound is  $5.37 \times 10^{-30}$  e.s.u which is 41 times that of standard NLO material urea ( $0.13 \times 10^{-30}$  e.s.u) [59]. The reported values of hyperpolarizability of quinoline derivatives are  $2.24 \times 10^{-30}$  and  $2.39 \times 10^{-30}$  e.s.u [60, 61].

The molecular second hyperpolarizability value can aid in gaining information about the physical properties of materials to understand the origin of third harmonic signals generated in chemical and biological structures. Such knowledge is effective in the development of optical devices including the application of optical communication, optical switching, optical signal processing and optical computing [62]. Measurement of the second hyperpolarizability values of compounds can provide insight into the molecular structural requirements for enhancement of third harmonic generation signal which has many application including Third harmonic generation microscopy for imaging biological structure by using contrast based on changes in the third-order nonlinear susceptibility which is a function of the molecular second hyperpolarizability [63, 64]. The average second hyperpolarizability has been calculated by using the following expression.

$$\gamma_{av} = 1/5[\gamma_{xxxx} + \gamma_{yyyy} + \gamma_{zzzz} + 2\gamma_{xxyy} + 2\gamma_{xxzz} + 2\gamma_{yyzz}]$$

The amount of charge transfer for the molecule depends on the nature of the end group of the molecule. Increase of  $\pi$ -conjugated chain length in organic molecules, in general, enhances the magnitude of hyperpolarizability. The calculated value of  $\gamma_{av}$  for the title compound is  $-2.833 \times 10^{-36}$  esu. The larger component of second hyperpolarizability is associated with the larger ground state polarization which leads to strong electronic coupling between the ground and the low lying excited state. This can be attributed to the enhanced charge transfer interaction taking place. Thus the present investigation provides a new route to design high performance NLO materials.

#### 4.7 Mulliken charges

The calculation of atomic charges plays an important role in the application of quantum mechanical calculations to molecular systems. Mulliken charges are calculated by determining the electron population of each atom as defined in the basis function. The charge distributions calculated by the Mulliken [65] and NBO methods for the equilibrium geometry

of 2-[(*E*)-2-bromophenyl ethynyl] quinoline-6-carboxylic acid are given in Table S2 (supporting material). The charge distribution on the molecule has an important influence on the vibrational spectra. Also we done a comparison of Mulliken charges obtained by different basis sets and tabulated it in Table S3 (supporting material) in order to assess the sensitivity of the calculated charges to changes in (i) the choice of the basis set; (ii) the choice of the quantum mechanical method. The results can, however, better be represented in graphical form as shown in Fig. S4 (supporting material). We have observed a change in the charge distribution by changing different basis sets. Distribution of the charges in this compound is also influenced by the carboxylic group and C<sub>26</sub>Br<sub>34</sub>. Based on the charge distribution calculated by various ways (see Tables S2 and S3) it can be concluded that all the hetero atoms showed significant electron density. An increased electron density (negative charge) can be also found in the neighbourhood of C<sub>4</sub>, C<sub>17</sub>, O<sub>12</sub>, C<sub>25</sub> and C<sub>26</sub>. Significantly positive charges were predicted for C<sub>3</sub> and C<sub>24</sub>. Therefore it can be concluded that electrophilic substitution of the quinoline scaffold is more preferred than nucleophilic substitution. Reactions based on the attack of a nucleophile are favoured especially on carboxyl carbons C<sub>10</sub> and C<sub>19</sub>.

#### 4.8. <sup>1</sup>H-NMR spectrum

The experimental spectrum data of title compound in DMSO is obtained at 500 MHz, using TMS as internal standard, and is shown in Table 4. B3LYP/GIAO was used to calculate the absolute isotropic chemical shielding of the title compound [66]. Relative chemical shifts were then estimated by using the corresponding TMS shielding:  $\sigma_{\text{calc}}(\text{TMS})$  calculated in advance at the same theoretical level as this paper. Numerical values of chemical shift  $\delta_{\text{calc}} = \sigma_{\text{calc}}(\text{TMS}) - \sigma_{\text{calc}}$  together with calculated values of  $\sigma_{\text{calc}}(\text{TMS})$ , are reported in Table 4. The chemical shift and the experimental <sup>1</sup>H NMR data were in agreement. Thus, the results have shown that the predicted proton chemical shifts were in good agreement with the experimental data for the title compound.

#### 4.8. Molecular docking

With time most microbes develop resistance against commercial antibiotics which increases the demand for development of new antimicrobial drugs. Oxo derivatives of Quinoline constitute a series of broad-spectrum antibacterial drugs [67]. In addition literature survey reveals that quinoline derivatives in general are highly active against different microbial strains [68-70]. Amongst the bacterial infections, tuberculosis (TB) is the leading bacterial infection in the world [71]. With the hypothesis that the quinoline derivative under study would be active against mycobacterium tuberculosis we decided to evaluate in silico antibacterial activity of the title compound. In addition to other molecular targets, the protein kinases have been recognized as effective molecular target in *Mycobacterium tuberculosis* drug discovery. In *Mycobacterium tuberculosis* the protein kinases genome contains 11 serine/threonine protein kinases, including protein kinase A (PknA) and protein kinase B (PknB), which play vital role in regulating cell shape and cell wall synthesis. PknB, is essential for mycobacterium viability and is predominant in many more distantly related gram-positive bacteria [72, 73]. PknB being an essential protein kinase has been established as molecular target for antibiotics [74] was selected as molecular target for docking.

Molecular docking simulations were performed on AutoDock-Vina software [75]. The 3D crystal structure of *M. tuberculosis* PknB was obtained from Protein Data Bank (PDB ID: 2FUM) [76]. The protein was prepared for docking by removing the co-crystallized ligand, water molecules and co-factors. AutoDockTools (ADT) graphical user interface was used to calculate Kollman charges and to add polar hydrogen. Ligand was prepared for docking by minimizing its energy at B3LYP/SDD level of theory. Charges were calculated by Geistenger method. Active site of the protein was defined in a way that it included residues of the active site within the grid dimensions of 40Å×40Å×40Å. The most popular

algorithm, Lamarckian Genetic Algorithm (LGA) available in Autodock Vina was employed for docking. Docking protocol was tested by redocking the co-crystallized inhibitor. Docking protocol which we employed predicted the same conformation as was present in the PDB crystal structure with RMSD value well within the reliable range of 2Å. Amongst the nine docked conformations, one which binded with high affinity at the active site was visualized for detailed ligand-protein interactions in Discover Studio Visualizer 4.0 and Pymol software.

The ligand binds at the catalytic site of substrate (Fig.S5-supporting material) by weak non-covalent interactions most prominent of which are H-bonding and alkyl- $\pi$  interactions. Asp156 forms two H-bonds of 2.27Å and 2.06Å lengths respectively with carboxylate oxygen. Met155, Ala38, Val25 Leu17 and Val95 hold the aromatic rings by alkyl-  $\pi$  interactions (given as supporting information in Fig. S6). The inhibitor 2-[(*E*)-2-(2-bromophenyl)ethenyl]quinoline-6-carboxylic acid forms a stable complex with PknB as is evident from the binding affinity ( $\Delta G$  in kcal/mol) values (supplementary Table S4). These preliminary results suggest that the compound might exhibit inhibitory activity against PknB. This may result in development of new anti-tuberculosic agents. However biological tests need to be done so as to validate computational predictions.

## 5. Conclusion

The FT-IR and FT-Raman studies of the title compound in the ground state were reported experimentally and theoretically. Potential energy distribution of normal modes of vibrations was done using GAR2PED program. The ring stretching modes in IR and Raman spectra are evidence for charge transfer interaction between the donor and the acceptor group through the  $\pi$  system. The chemical reactivity is understood from chemical potential, electrophilicity and global hardness. MEP predicts the most reactive part in the molecule. Optimized geometrical parameters of the title compound are in agreement with that of similar derivatives. The calculated first hyperpolarizability is comparable with the reported values of similar quinoline derivatives and the study of second hyperpolarizability reveals it is an attractive compound for future studies in non linear optics. The calculated  $^1\text{H-NMR}$  results are in good agreement with the experimental data. The molecular docking results suggest that the compound might exhibit inhibitory activity against PknB and this may result in development of new anti-tuberculosic agents.

## Acknowledgements

The authors are thankful to University of Antwerp for access to the university's CalcUA Supercomputer Cluster. RTU thanks University of Kerala for a research fellowship and JAW would like to thank Department of Science and Technology, New Delhi, India for INSPIRE fellowship.

## References

- [1] F. Hayat, A. Salahuddin, S. Umar, A. Azam, *Eur. J. Med. Chem.* 45 (2010) 4669-4675.
- [2] L.M. Bedoya, M.J. Abad, E. Calonge, L.A. Saavedra, C.M. Gutierrez, V.V. Kouznetsov, J. Alcamí, P. Bermejo, *Antivir. Res.* 87 (2010) 338-344.
- [3] A.M. Asiri, A.O. Baglaf, R.M. Abdel-Rahman, S.A. Khan, M. Ishaq, *Asian J. Chem.* 25 (2013) 7779-7782.
- [4] S.A. Khan, A.M. Asiri, K. Sharma, *Med. Chem. Res.* 22 (2013) 1998-2004
- [5] M.V.N. Souza, K.C. Pais, C.R. Kaiser, M.A.L. Peralta, M.L. Ferreira, M.C.S. Lourenço, *Bioorg. Med. Chem.* 17 (2009) 1474-1480.
- [6] R.K. Arafa, G.H. Hegazy, G.A. Piazza, A.H. Abadi, *Eur. J. Med. Chem.* 63 (2013) 826-832.
- [7] M.G. Ferlin, B. Gatto, G. Chiarelto, M. Palumbo, *Bioorg. Med. Chem.* 8 (2000)1415-1422.

- [8] N. Chowdhury, M. Angopadhyay, S. Karthik, N.D.P. Singh, M. Baidya, S.K.Ghosh, *J. Photo. Chem. Photo. Biol. B* 130 (2014) 188-198.
- [9] M.P. Bernstein, A.L. Mattioda, S.A. Sandford, D.M. Hudgins, *Astrophys. J.* 626 (2005) 909-918
- [10] A. Spalletti, *Photochem. Photobiol. Sci.* 3 (2004) 695-699.
- [11] Z. He, G.H.W. Milburn, K.J. Baldwin, D.A. Smith, A. Danel, P. Tomasik, *J. Lumin.* 86 (2000) 1-14.
- [12] Y.T. Tao, E. Balasubramanian, A. Danel, B. Jarosz, P. Tomasik, *Appl. Phys. Lett.* 77 (2000) 1575-1577.
- [13] J. Niziol, A. Danel, G. Boiteux, J. Davenas, B. Jarosz, A. Wisla, G. Seytre, *Synth. Met.* 127 (2002) 175-180.
- [14] A. Mousnier, H. Leh, J.F. Mouscadet, C. Dargemont, *Mol. Pharmacol.* 66 (2004) 783-788.
- [15] S. Bonnenfant, C.M. Thomas, C. Vita, F. Subra, E. Deprez, F. Zouhri, D. Desmaële, J. D'Angelo, J.F. Mouscadet, H. Leh, *J. Virol.* 78 (2004) 5728-5736.
- [16] A.G. MacDiarmid, A.J. Epstein, in: S.A. Jenekhe, K.J. Wynne (Eds.), *Photonic and Optoelectronic Polymers*, Am. Chem. Soc. Washington DC 1997, p. 395.
- [17] A.J. Epstein, *Mater. Res. Soc. Bull.* 22 (1997) 16-24.
- [18] T.K. Khan, M. Ravikanth, *Dyes Pigm.* 95 (2012) 89-95
- [19] E. Inkaya, S. Gunnaz, N. Ozdemir, O. Dayan, M. Dinçer, B. Cetinkaya, *Sepetrochim. Acta Part A* 103 (2013) 255-263.
- [20] B. Podeszawa, H. Niedbala, J. Polanski, R. Musiol, D. Tabak, J. Finster, K. Serafin, M. Milczarek, J. Wietrzyk, S. Boryczka, W. Mol, J. Jampilek, J. Dohnal, D.S. Kalinowski, D.R. Richardson, *Bioorg. Med. Chem. Lett.* 17 (2007) 6238-6141.
- [21] R. Musiol, J. Jampilek, K. Kralova, D.R. Richardson, D. Kalinowski, B. Podeszawa, J. Finster, H. Niedbala, A. Palka, J. Polanski, *Bioorg. Med. Chem.* 105 (2007) 1280-1288.
- [22] Gaussian 09, Revision B.01, M. J. Frisch, G. W. Trucks, H. B. Schlegel, G. E. Scuseria, M. A. Robb, J. R. Cheeseman, G. Scalmani, V. Barone, B. Mennucci, G. A. Petersson, H. Nakatsuji, M. Caricato, X. Li, H. P. Hratchian, A. F. Izmaylov, J. Bloino, G. Zheng, J. L. Sonnenberg, M. Hada, M. Ehara, K. Toyota, R. Fukuda, J. Hasegawa, M. Ishida, T. Nakajima, Y. Honda, O. Kitao, H. Nakai, T. Vreven, J. A. Montgomery, Jr., J. E. Peralta, F. Ogliaro, M. Bearpark, J. J. Heyd, E. Brothers, K. N. Kudin, V. N. Staroverov, T. Keith, R. Kobayashi, J. Normand, K. Raghavachari, A. Rendell, J. C. Burant, S. S. Iyengar, J. Tomasi, M. Cossi, N. Rega, J. M. Millam, M. Klene, J. E. Knox, J. B. Cross, V. Bakken, C. Adamo, J. Jaramillo, R. Gomperts, R. E. Stratmann, O. Yazyev, A. J. Austin, R. Cammi, C. Pomelli, J. W. Ochterski, R. L. Martin, K. Morokuma, V. G. Zakrzewski, G. A. Voth, P. Salvador, J. J. Dannenberg, S. Dapprich, A. D. Daniels, O. Farkas, J. B. Foresman, J. V. Ortiz, J. Cioslowski, and D. J. Fox, Gaussian, Inc., Wallingford CT, 2010.
- [23] J.B. Foresman, in: E. Frisch (Ed.), *Exploring Chemistry with Electronic Structure Methods: A Guide to Using Gaussian*, Gaussian, Inc., Pittsburg, PA, 1996.
- [24] P.J. Hay, W.R. Wadt, *J. Chem Phys.* 82 (1985) 270-283.
- [25] J. Zhao, Y. Zhang, L. Zhu, *J. Mol. Struct. Theochem.* 671 (2004) 179-187.
- [26] GaussView, Version 5, R. Dennington, T. Keith, J. Millam, Semichem Inc., Shawnee Mission KS, 2009.
- [27] J.M.L. Martin, C.V. Alsenoy, GAR2PED, A Program to Obtain a Potential Energy Distribution from a Gaussian Archive Record, University of Antwerp, Belgium, 2007.
- [28] N.P.G Roeges, *A guide to the complete interpretation of IR spectra of Organic Compounds*, Wiley, New York 1994.

- [29] J.B. Bhagyasree, H.T. Varghese, C.Y. Panicker, J. Samuel, C.V. Alsenoy, K. Bolelli, I. Yildiz, E. Aki, *Spectrochim. Acta* 102 (2013) 99-113.
- [30] R.T. Ulahannan, C.Y. Panicker, H.T. Varghese, C. V. Alsenoy, R. Musiol, J.Jampilek, P.L. Anto, *Spectrochim. Acta Part A* 121 (2014) 404-414
- [31] Y.S. Mary, H.T. Varghese, C.Y. Panicker, T.Ertan, I. Yildiz, O. Temiz-Arpaci, *Spectrochim. Acta Part A* 71 (2008) 566-571.
- [32] G. Varsanyi, *Assignments of Vibrational Spectra of Seven Hundred Benzene Derivatives*, Wiley, New York 1974.
- [33] J. Coates, R.A. Meyers, *Encyclopedia of Analytical Chemistry*, John Wiley and Sons, Chichester , Vol. 12, 2000.
- [34] G. Socrates, *Infrared Characteristic Group Frequencies*, John Wiley and Sons, New York, 1981.
- [35] H.T. Varghese, C.Y. Panicker, K.M. Pillai, M.Y. Sheena, K. Raju, T.K. Manojkumar, A. Bielenica, C.V. Alsenoy, *Spectrochim. Acta Part A* 76 (2010) 513-522
- [36] J. Chowdhury, M. Ghosh, T.N. Misra, *Spectrochim. Acta* 56 (2000) 2107-2115
- [37] H.T Varghese, C.Y Panicker, D. Philip, *J. Raman Spectrosc.* 38 (2007) 309-315
- [38] Y.S. Mary, H.T. Varghese, C.Y. Panicker, M. Dolezal, *Spectrochim. Acta* 71 (2008) 725-730.
- [39] H.T Varghese, C.Y Panicker, D. Philip, *J. Raman Spectrosc.* 38 (2007) 309-315
- [40] V. Arjunan, S.T. Govindaraja, A. Jayapraksh, S. Mohan, *Spectrochim. Acta* 107 (2013) 62-71.
- [41] S.R. Sheeja, N.A. Mangalam, M.R.P. Kurup, Y.S. Mary, K. Raju , H.T.Varghese, C.Y. Panicker, *J. Mol. Struct.* 973 (2010) 36-46 .
- [42] M. Sacmaci, H.K. Cavus, H. Ari, R. ShingoZ, T. Ozpazan , *Spectrochim. Acta* 97 (2012) 88-99.
- [43] N. Sinha, O. Prasad, V. Narayan, S.R. Shukla, *J. Mol. Simul.* 37 (2011) 153-163.
- [44] D.F.V. Lewis, C. Loannides, D.V. Parke, *Xenobiotica* 24 (1994) 401-408.
- [45] B. Kosar, C. Albayrak, *Spectrochim. Acta A* 78 (2011) 160-167.
- [46] K. Fukui, *Science* 218 (1982) 747-754.
- [47] T.A. Koopmans, *Physica* 1 (1993) 104-113
- [48] R.J. Parr, R.G. Pearson, *J. Am. Chem. Soc.* 105 (1983) 7512-7516.
- [49] E. Scrocco, J. Tomasi, *Adv. Quantum. Chem.* 103 (1978) 115 -193.
- [50] F.J. Luque, J.M. Lopez, M. Orozco, *Theor. Chem. Acc.* 103 (2000) 343-345.
- [51] P. Politzer, J.S. Murray, in: *Theoretical Biochemistry and Molecular Biophysics: A Comprehensive Survey*, Vol. 2, Protein. D.L. Beveridge, R.Lavery, Eds., Adenine Press, Schenectady, NY, 1991, Chap. 13.
- [52] E. Scrocco, J. Tomasi, *Top. Curr. Chem.* 42 (1973) 95-170.
- [53] NBO Version 3.1, E.D. Glendening, A.E. Reed, J.E. Carpenter, and F. Weinhold
- [54] J. Choo, S. Kim, H. Joo, Y. Kwon, *J. Mol. Struct. (Theochem.)* 587 (2002) 1-8.
- [55] Y.R. Shen, *The Principles of Nonlinear Optics*, Wiley, New York, 1984.
- [56] P.V. Kolinsky, *Opt. Eng.* 31 (1992) 1676-1684.
- [57] D.F. Eaton, *Science* 25 (1991) 281-287.
- [58] D.A. Kleinman, *Phys. Rev.* 126 (1962) 1977- 1979.
- [59] M. Adant, M. Dupuis, J.L. Bredas, *Int. J. Quantum. Chem.* 56 (1995) 497-507.
- [60] G. Purohit, G.C. Joshi, *Indian J. Pure Appl. Phys.* 41 (2003) 922-927.
- [61] A.J. Camargo, H.B. Napolitano, J. Zukerman-Schpector, *J. Mol. Struct. (Theochem.)* 816 (2007) 145-151.
- [62] D. Tokarz, R. Cisek, N. Prent, U. Fekl, V. Barzda, *Analytica Chimica Acta* 755 (2012) 86-92.

- [63] R. Cisek, L. Spencer, N. Prent, D. Zigmantas, G. Espie, V. Barzda, *Photosynth. Res.* 102 (2009) 111-141.
- [64] W.J. Nie, *Adv. Mater.* 5 (1993) 520-545
- [65] R.S. Mulliken, *J. Chem. Phys.*, 23 (1955) 1833-1840
- [66] K. Wolinski, J.F. Hinton, P. Pulay, *J. Am. Chem. Soc.* 112 (1990) 8251-8260.
- [67] M.I. Andersson, A.P. MacGowan, *J. Antimicrob. Chemother.* 51 (2003) 1-11.
- [68] R. Wise, J.M. Andrews, J.P. Ashby, R.S. Matthews, *Antimicrob. Agents Chemother.* 32 (1988) 617-622.
- [69] H.C. Neu, *Annual Rev. Med.* 43 (1992) 465-486.
- [70] M.J. Pucci, J.A. Wiles, *Bacterial Topoisomerase Inhibitors: Quinolones and Beyond*, In *Antimicrobials*, ch.16, pp. 307-326, Springer Berlin, Heidelberg, 2014.
- [71] M. Chhabria, P. Shailesh, J. Mitesh, *Anti-Infect. Agents Med. Chem.* 9 (2010) 59-103.
- [72] C.M. Kang, D.W. Abbott, S.T. Park, C.C. Dascher, L.C. Cantley, R.N. Husson, *Genes Dev.* 19 (2005) 1692-1704.
- [73] P. Fernandez, B. Saint-Joanis, N. Barilone, M. Jackson, B. Gicquel, S.T. Cole, P.M. Alzari, *J. Bacteriol.* 188 (2006) 7778-7784.
- [74] K.E.A. Lougheed, S.A. Osborne, B. Saxty, D. Whalley, T. Chapman, N. Bouloc, J. Chugh, T.J. Nott, D. Patel, V.L. Spivey, C.A. Kettleborough, J.S. Bryans, D.L. Taylor, S.J. Smerdon, R.S. Buxton, *Tuberculosis* 91 (2011) 277-286.
- [75] O. Trott, A. J. Olson, *J. Comput. Chem.* 31 (2010) 455-461.
- [76] A. Wehenkel, P. Fernandez, M. Bellinzoni, V. Catherinot, N. Barilone, G. Labesse, M. Jackson, P.M. Alzari, *FEBS Lett.* 580 (2006) 3018-3022.

#### Figure Captions

Fig.1 FT-IR spectrum of 2-[(*E*)-2-(2-bromophenyl)ethenyl]quinoline-6-carboxylic acid

Fig.2 FT-Raman spectrum of 2-[(*E*)-2-(2-bromophenyl)ethenyl]quinoline-6-carboxylic acid

Fig.3 Optimized geometry (B3LYP/SDD) of 2-[(*E*)-2-(2-bromophenyl)ethenyl]quinoline-6-carboxylic acid

Fig.4 HOMO and LUMO plots of 2-[(*E*)-2-(2-bromophenyl)ethenyl]quinoline-6-carboxylic acid

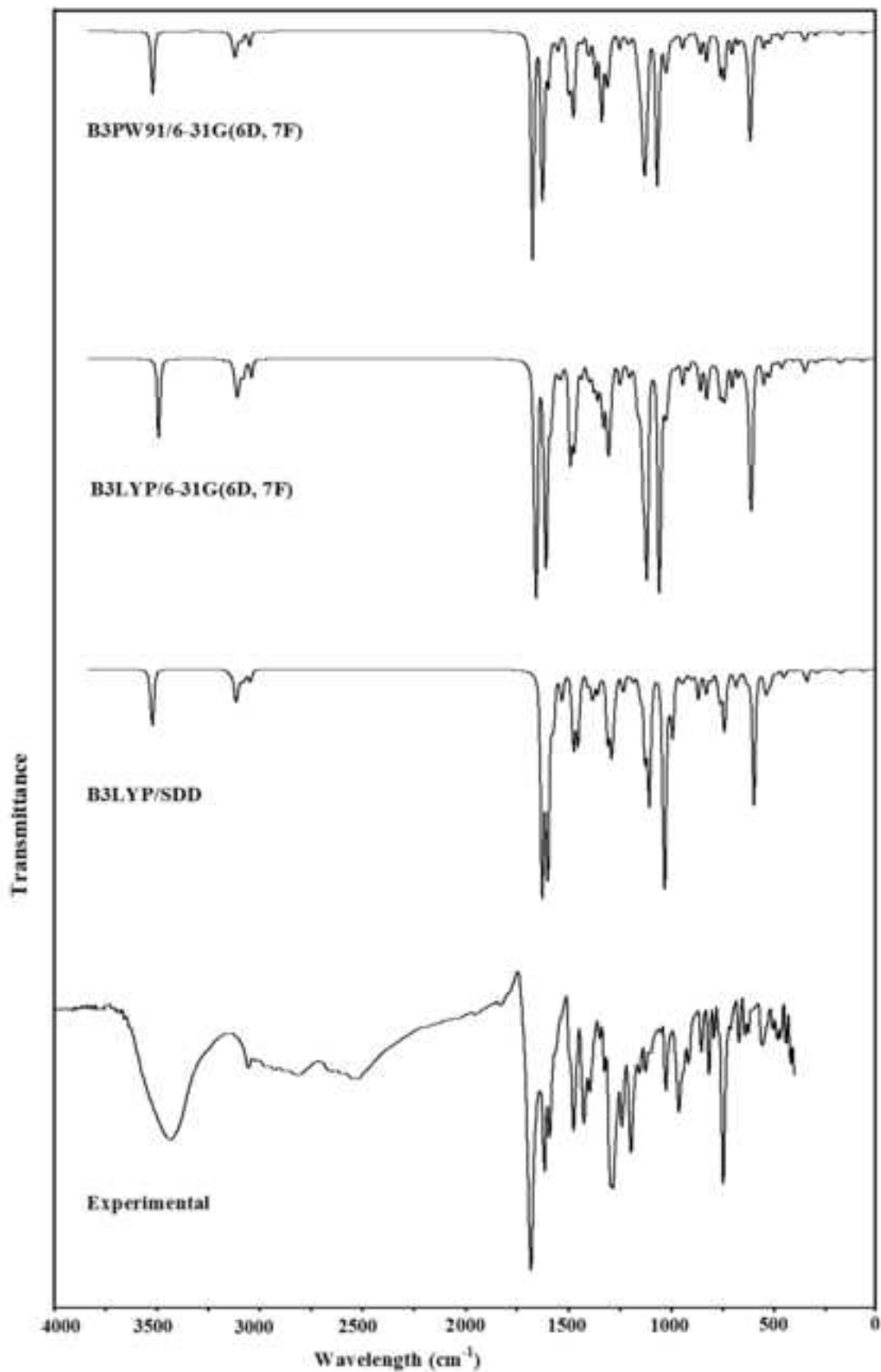


Fig.1 FT-IR spectrum of  
2-[(*E*)-2-(2-bromophenyl)ethenyl]quinoline-6-carboxylic acid

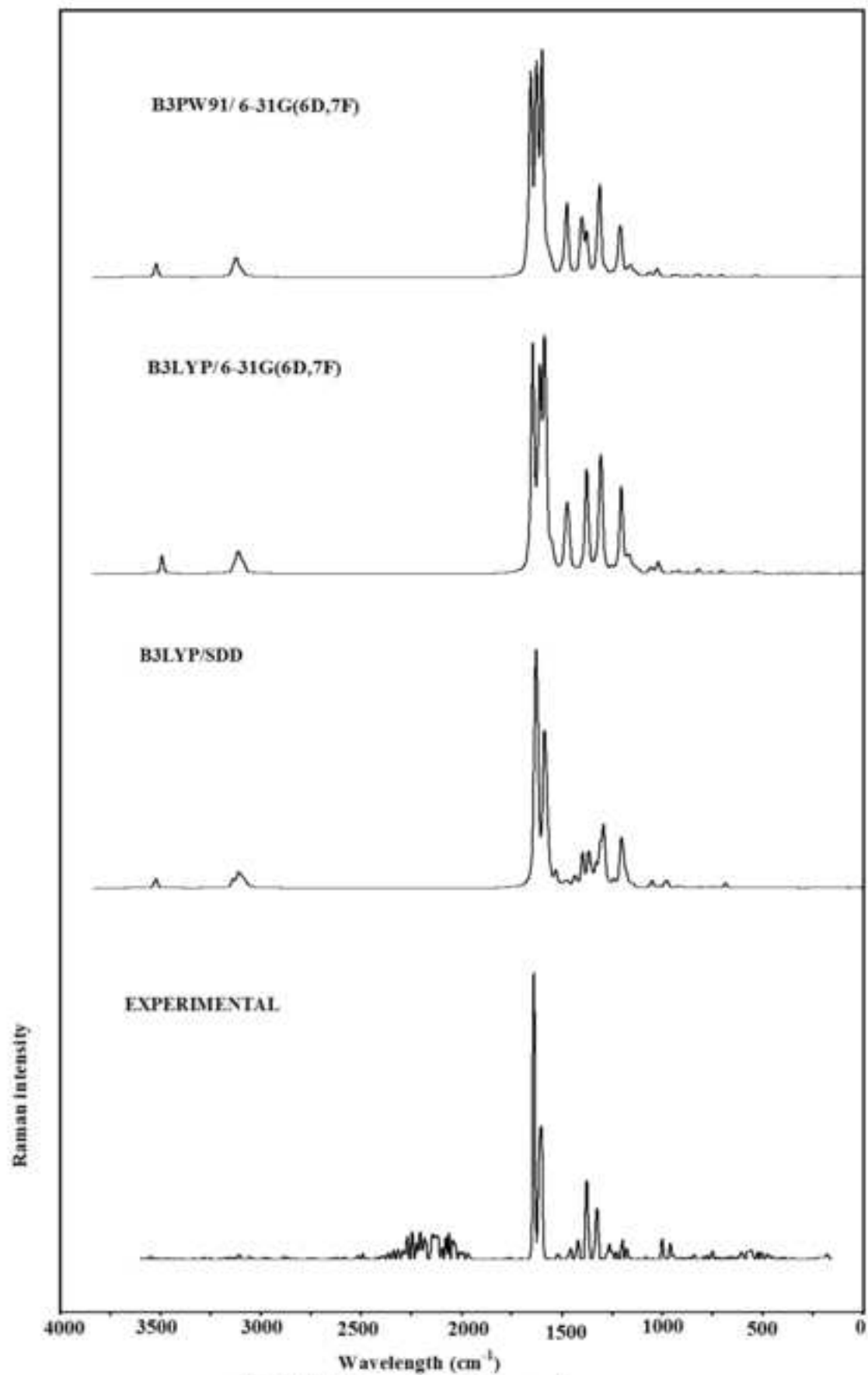
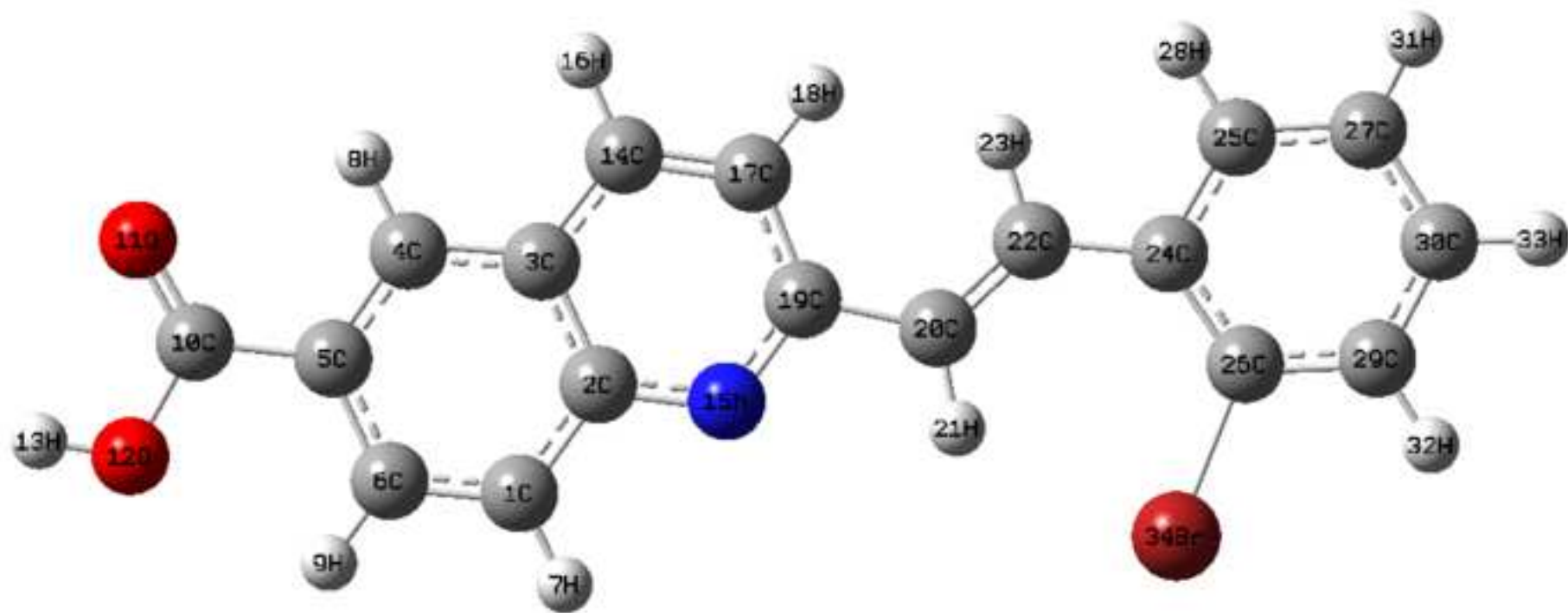
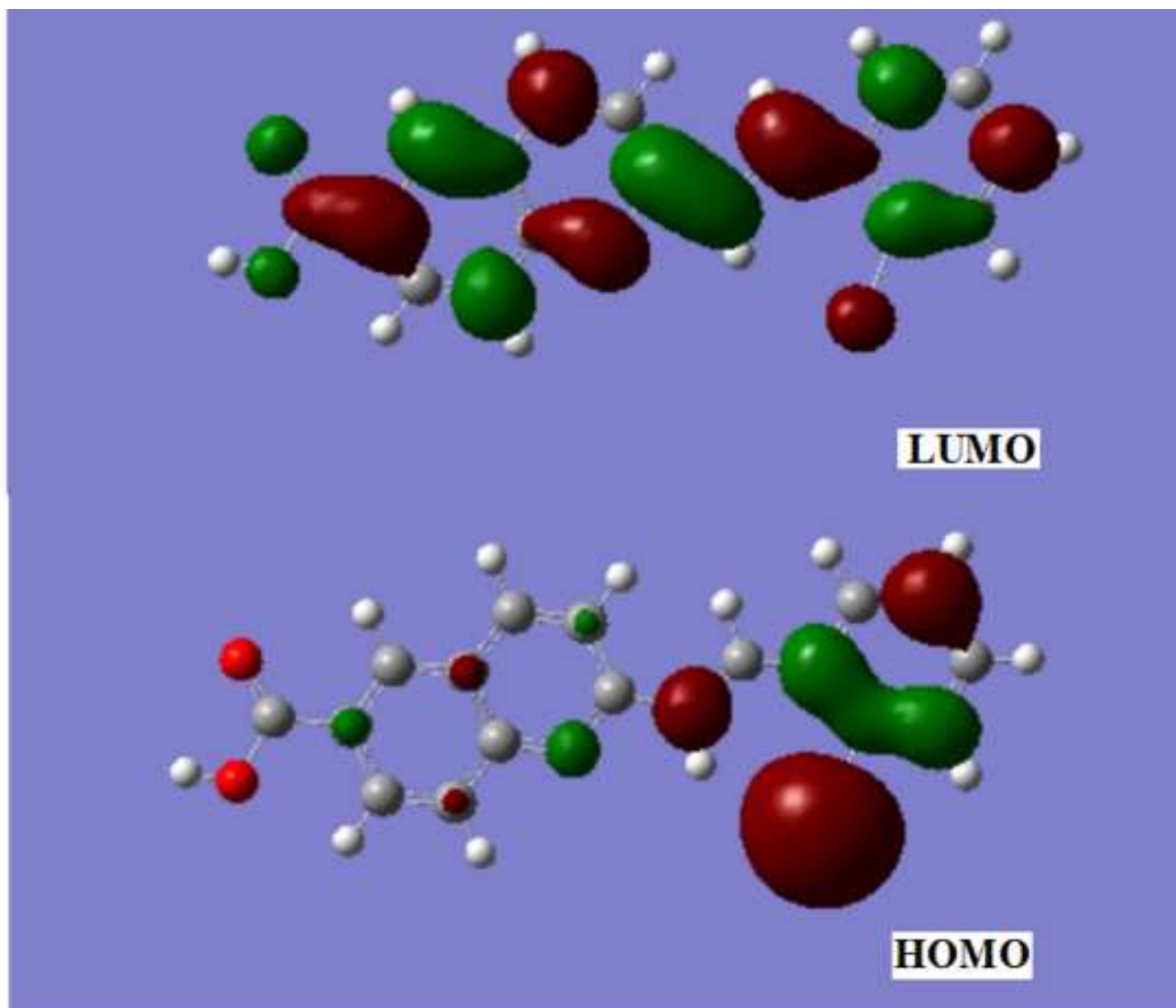


Fig.2 FT-Raman spectrum of  
2-[(E)-2-(2-bromophenyl)ethenyl]quinoline-6-carboxylic acid



**Fig.3 Optimized geometry (B3LYP/SDD) of 2-[(*E*)-2-(2-bromophenyl)ethenyl]quinoline-6-carboxylic acid**



**Fig.4 HOMO and LUMO plots of 2-[(*E*)-2-(2-bromophenyl)ethenyl]quinoline-6-carboxylic acid**

Table 1. Optimized geometrical parameters (B3LYP/SDD) of 2ebq6c, atom labelling according to Fig.3.

<u>Bond lengths (Å)</u>		<u>Bond angles (°)</u>		<u>Dihedral angles (°)</u>	
C1-C2	1.4290	C2-C1-C6	120.6	C6-C1-C2-C3	0.0
C1-C6	1.3862	C2-C1-H7	117.7	C6-C1-C2-N15	-180.0
C1-H7	1.0853	C6-C1-H7	121.8	H7-C1-C2-C3	-180.0
C2-C3	1.4418	C1-C2-C3	119.1	H7-C1-C2-N15	0.0
C2-N15	1.3772	C1-C2-N15	118.6	C2-C1-C6-C5	0.0
C3-C4	1.4197	C3-C2-N15	122.3	C2-C1-C6-H9	180.0
C3-C14	1.4322	C2-C3-C4	119.5	H7-C1-C6-C5	-180.0
C4-C5	1.3958	C2-C3-C14	117.2	H7-C1-C6-H9	0.0
C4-H8	1.0872	C4-C3-C14	123.3	C1-C2-C3-C4	0.0
C5-C6	1.4317	C3-C4-C5	120.3	C1-C2-C3-C14	180.0
C5-C10	1.4834	C3-C4-H8	120.5	N15-C2-C3-C4	180.0
C6-H9	1.0843	C5-C4-H8	119.1	N15-C2-C3-C14	0.0
C10-O11	1.2452	C4-C5-C6	120.3	C1-C2-N15-C19	-180.0
C10-O12	1.3912	C4-C5-C10	118.2	C3-C2-N15-C19	0.0
O12-H13	0.9837	C6-C5-C10	121.5	C2-C3-C4-C5	0.0
C14-H16	1.0876	C1-C6-C5	120.2	C2-C3-C4-H8	-180.0
C14-C17	1.3818	C1-C6-H9	121.0	C14-C3-C4-C5	180.0
N15-C19	1.3499	C5-C6-H9	118.7	C14-C3-C4-H8	0.0
C17-H18	1.0843	C5-C10-O11	125.9	C2-C3-C14-H16	180.0
C17-C19	1.4423	C5-C10-O12	112.9	C2-C3-C14-C1	0.0
C19-C20	1.4724	O11-C10-O12	121.2	C4-C3-C14-H16	0.0
C20-H21	1.0817	C10-O12-H13	110.2	C4-C3-C14-C17	-180.0
C20-C22	1.3619	C3-C14-H16	119.4	C3-C4-C5-C6	0.0
C22-H23	1.0903	C3-C14-C17	119.8	C3-C4-C5-C10	-180.0
C22-C24	1.4745	H16-C14-C17	120.7	H8-C4-C5-C6	180.0
C24-C25	1.4287	C2-N15-C19	119.4	H8-C4-C5-C10	0.0
C24-C26	1.4233	C14-C17-H18	120.1	C4-C5-C6-C1	0.0
C25-C27	1.3991	C14-C17-C19	119.8	C4-C5-C6-H9	180.0
C25-H28	1.088	H18-C17-C19	120.1	C10-C5-C6-C1	180.0
C26-C29	1.4057	N15-C19-C17	121.5	C10-C5-C6-H9	0.0
C26-Br34	1.9693	N15-C19-C20	114.8	C4-C5-C10-O11	0.0
C27-C30	1.4072	C17-C19-C20	123.6	C4-C5-C10-O12	180.0
C27-H31	1.0865	C19-C20-H21	112.8	C6-C5-C10-O11	-180.0
C29-C30	1.4055	C19-C20-C22	125.0	C6-C5-C10-O12	0.0
C29-H32	1.0853	H21-C20-C22	122.1	C5-C10-O12-H13	-180.0
C30-H33	1.0864	C20-C22-H23	116.8	O11-C10-O12-H13	0.0
		C20-C22-C24	131.7	C3-C14-C17-H18	180.0
		H23-C22-C24	111.4	C3-C14-C17-C19	0.0
		C22-C24-C25	114.8	H16-C14-C17-H18	0.0
		C22-C24-C26	129.7	H16-C14-C17-C19	-180.0
		C25-C24-C26	115.4	C2-N15-C19-C17	0.0
		C24-C25-C27	123.1	C2-N15-C19-C20	-180.0

C24-C25-H28	117.7	C14-C17-C19-N15	0.0
C27-C25-H28	119.1	C14-C17-C19-C20	180.0
C24-C26-C29	122.0	H18-C17-C19-N15	-180.0
C24-C26-Br34	123.7	H18-C17-C19-C20	0.0
C29-C26-Br34	114.2	C15-C19-C20-H21	0.0
C25-C27-C30	119.5	C15-C19-C20-C22	-180.0
C25-C27-H31	119.9	C17-C19-C20-H21	-180.0
C30-C27-H31	120.5	C17-C19-C20-C22	0.0
C26-C29-C30	120.5	C19-C20-C22-H23	0.0
C26-C29-H32	119.5	C19-C20-C22-C24	180.0
C30-C29-H32	119.9	H21-C20-C22-H23	-180.0
C27-C30-C29	119.3	H21-C20-C22-C24	-0.0
C27-C30-H33	120.9	C20-C22-C24-C25	-180.0
C29-C30-H33	119.8	C20-C22-C24-C26	0.0
		H23-C22-C24-C25	0.0
		H23-C22-C24-C26	-180.0
		C22-C24-C25-C27	180.0
		C22-C24-C25-H28	0.0
		C26-C24-C25-C27	-0.0
		C26-C24-C25-H28	180.0
		C22-C24-C26-C29	-180.0
		C22-C24-C26-Br34	0.0
		C25-C24-C26-C29	0.0
		C25-C24-C26-Br34	-180.0
		C24-C25-C27-C30	-0.0
		C24-C25-C27-H31	-180.0
		H28-C25-C27-C30	180.0
		H28-C25-C27-H31	0.0
		C24-C26-C29-C30	0.0
		C24-C26-C29-H32	-180.0
		Br34-C26-C29-C30	180.0
		Br34-C26-C29-H32	-0.0
		C25-C27-C30-C29	0.0
		C25-C27-C30-H33	180.0
		H31-C27-C30-C29	-180.0
		H31-C27-C30-H33	-0.0
		C26-C29-C30-C27	-0.0
		C26-C29-C30-H33	180.0
		H32-C29-C30-C27	180.0
		H32-C29-C30-H33	0.0

Table 2. Calculated wavenumbers (Scaled), observed IR, Raman bands and assignments of 2-[(*E*)-2-(2-bromophenyl)ethenyl]quinoline-6-carboxylic acid

B3PW91/6-31G(6D, 7F)			B3LYP/6-31G(6D, 7F)			B3LYP/SDD			IR	Raman	Assignments <sup>a</sup>
$\nu(\text{cm}^{-1})$	IR <sub>I</sub>	R <sub>A</sub>	$\nu(\text{cm}^{-1})$	IR <sub>I</sub>	R <sub>A</sub>	$\nu(\text{cm}^{-1})$	IR <sub>I</sub>	R <sub>A</sub>	$\nu(\text{cm}^{-1})$	$\nu(\text{cm}^{-1})$	-
3661	87.33	331.69	3489	73.66	348.32	3522	93.23	277.64	-	-	$\nu\text{OH}(100)$
3298	1.67	23.42	3169	1.91	23.45	3147	4.75	16.80	-	-	$\nu\text{CH}(99)$
3265	2.54	161.71	3130	2.97	163.03	3130	2.80	146.19	-	-	$\nu\text{CHI}(82)$ $\nu\text{CHII}(17)$
3253	17.90	293.95	3117	16.82	266.02	3118	26.36	314.41	-	-	$\nu\text{CHII}(75)$ $\nu\text{CHII}(19)$
3245	12.79	79.96	3109	13.89	81.50	3115	12.81	61.18	-	-	$\nu\text{CH}(99)$
3244	1.09	49.66	3108	1.73	51.55	3106	1.40	40.31	-	-	$\nu\text{CHI}(99)$
3239	16.76	169.69	3102	21.69	219.06	3103	18.16	135.24	-	-	$\nu\text{CHII}(98)$
3227	0.62	66.93	3094	0.99	67.89	3091	0.86	61.86	-	-	$\nu\text{CHI}(99)$
3224	1.31	104.98	3088	8.39	114.32	3087	6.67	85.94	-	-	$\nu\text{CHII}(94)$
3214	5.03	59.15	3078	5.39	56.58	3079	4.72	46.97	-	-	$\nu\text{CH}(98)$
3207	8.46	46.66	3073	9.23	50.80	3071	12.12	44.21	-	-	$\nu\text{CHII}(94)$
3170	18.73	23.94	3039	18.16	22.49	3044	19.43	18.74	3057	3045	$\nu\text{CH}(97)$
1739	304.8	355.34	1657	293.58	377.29	1627	120.32	3539.9	-	1634	$\nu\text{CO}(74)$
1718	0.33	4876.9	1641	1.07	5014.5	1623	175.26	1788.9	1616	1618	$\nu\text{C}=\text{C}(49)$ $\delta\text{CH}(23)$

1687	263.4	5486.0	1609	256.30	4779.9	1600	347.22	7632.8	-	1593	$\nu$ PhI(63) $\nu$ PhI(20)
1664	6.55	1525.0	1586	14.01	803.36	1574	46.91	5.23	1588	-	$\nu$ PhII(31) $\nu$ C=C(15)
1658	64.33	4397.3	1582	62.27	5313.6	1568	29.47	6476.4	1563	1560	$\nu$ C=C(24) $\nu$ PhII(26)
1626	8.02	490.21	1551	7.48	480.63	1537	8.25	512.10	1534	-	$\nu$ PhII(72) $\delta$ CHII(14)
1610	19.79	174.08	1535	16.69	131.22	1527	31.69	269.02	-	1500	$\nu$ PhI(41) $\nu$ CC(15) $\nu$ C=N(24)
1557	91.80	149.58	1488	93.21	84.495	1474	111.83	234.94	1476	-	$\nu$ PhI(42) $\delta$ CH(12) $\nu$ CC(21)
1542	36.77	332.57	1477	19.00	688.69	1453	72.02	20.97	-	1463	$\delta$ CHII(22) $\nu$ PhII(42)
1532	99.83	1689.2	1467	100.38	1501.1	1446	35.40	2029.91	-	1437	$\nu$ PhI(12) $\delta$ CHI(20) $\delta$ CH(12) $\nu$ C=N(10)
1493	14.84	53.92	1434	14.82	39.98	1402	16.74	54.79	1421	1396	$\delta$ CHII(25) $\nu$ PhII(56)

1459	17.11	730.73	1398	24.32	83.93	1383	23.57	830.11	1392	1385	$\delta$ CH(16) $\nu$ PhI(51)
1451	17.26	902.45	1377	10.22	737.22	1375	17.47	971.10	-	-	$\nu$ PhI(67)
1428	6.25	1100.3	1371	22.00	1875.8	1356	24.09	1218.64	-	-	$\delta$ CH(35) $\nu$ PhI(17)
1420	51.36	20.96	1354	31.04	5.99	1341	8.84	91.74	1345	1347	$\nu$ C=N(17) $\nu$ C=C(10) $\delta$ CH(10)
1392	117.65	20.31	1330	74.24	159.87	1308	72.03	180.18	1323	1314	$\delta$ OH(63) $\delta$ CHI(12) $\delta$ CH(11)
1379	12.78	127.27	1308	0.85	46.53	1300	22.40	113.15	1296	-	$\nu$ PhII(80)
1363	78.55	2797.5	1303	121.39	3339.0	1285	119.34	3397.33	1281	1285	$\nu$ CN(38), $\nu$ CO(25)
1348	23.87	2.63	1291	19.96	3.52	1272	21.17	34.39	-	-	$\nu$ CO(45) $\delta$ CHII(35)
1332	0.33	136.23	1279	1.58	25.49	1259	3.13	74.26	-	-	$\nu$ CN(14) $\delta$ CHI(35) $\delta$ Ring(11)
1299	14.84	60.56	1248	11.95	78.77	1234	19.53	155.16	1236	1239	$\delta$ CHI(14) $\nu$ PhI(55)

1297	7.25	3.56	1245	3.52	22.16	1227	12.89	36.12	-	-	$\delta$ CHII(30) $\delta$ CH(35)
1274	2.36	171.23	1213	25.49	208.68	1204	4.52	168.50	-	1205	$\nu$ CC(28) $\nu$ PhI(22) $\delta$ CH(11)
1255	19.04	1724.3	1200	78.77	1762.1	1184	12.94	1557.20	1196	-	$\nu$ CC(34) $\nu$ PhII(25) $\delta$ CHII(20)
1224	2.30	84.34	1176	4.09	209.43	1160	6.53	234.58	1154	1158	$\delta$ CHII(69) $\nu$ PhII(10)
1204	56.38	353.14	1159	56.67	378.82	1146	34.36	274.77	-	-	$\delta$ CH(43) $\delta$ CHI(51)
1184	152.00	129.03	1137	109.16	116.57	1123	107.94	150.20	1123	1117	$\delta$ CHI(39) $\nu$ PhI(12) $\delta$ OH(10)
1171	11.54	12.73	1121	11.71	10.24	1104	20.22	9.27	1098	-	$\nu$ PhII(54) $\delta$ CHII(41)
1166	200.19	48.44	1118	239.34	64.75	1103	116.03	66.70	-	-	$\delta$ OH(23) $\nu$ CC(12)
1107	252.21	96.00	1054	279.00	104.65	1032	349.46	133.32	1047	1045	$\nu$ CO(39) $\delta$ OH(17)

1097	4.19	51.31	1050	4.67	49.41	1031	3.64	109.47	1023	1023	$\nu$ PhII(22) $\delta$ CHII(60)
1065	30.09	0.99	1026	35.35	0.16	1006	4.87	0.34	-	-	$\tau$ C=O(31) $\gamma$ CH(57)
1064	33.81	253.15	1016	33.89	284.19	1005	33.52	0.40	-	-	$\nu$ PhII(20) $\delta$ PhII(43)
1054	14.80	5.02	1009	3.31	6.33	993	0.33	1.00	-	-	$\gamma$ CHII(73) $\tau$ PhII(17)
1037	0.01	0.55	994	0.05	0.73	990	45.17	264.79	-	-	$\gamma$ CHI(86)
1026	0.01	0.55	994	0.05	0.73	990	24.76	2.53	-	-	$\gamma$ PhI(51) $\gamma$ CH(28)
1013	1.78	7.60	969	2.53	8.59	960	0.30	0.22	960	965	$\gamma$ CHII(72)
985	6.32	2.26	944	8.21	3.92	946	17.86	3.28	942	-	$\delta$ Ring(27) $\delta$ PhI(23)
981	16.42	1.83	942	15.13	4.20	930	9.47	4.53	-	929	$\gamma$ CHI(70) $\tau$ PhI(10)
980	1.30	32.61	939	0.37	30.32	911	0.00	23.12	912	-	$\gamma$ CH(51) $\gamma$ CHII(26)
957	7.72	58.06	915	10.12	63.59	900	14.44	72.46	-	-	$\delta$ PhI(17) $\gamma$ OH(41) $\nu$ CC(10)
921	0.47	2.40	882	0.49	2.43	868	34.83	0.36	-	-	$\gamma$ CHII(68)

908	2.96	24.79	870	3.72	25.64	865	4.60	2.58	-	-	$\delta$ CC(21) $\delta$ PhII(20) $\delta$ CH(14) $\nu$ CC(12)
892	32.51	1.57	856	28.25	1.91	852	2.93	19.88	852	-	$\gamma$ CHI(69)
861	35.56	1.45	827	31.22	1.60	829	33.78	1.92	-	836	$\gamma$ CH(43) $\gamma$ PhI(27)
854	8.95	87.12	817	10.73	89.12	803	6.46	0.49	813	-	$\delta$ Ring(39) $\nu$ PhI(16)
827	2.66	1.40	793	3.65	1.75	802	11.01	101.82	-	-	$\delta$ Ring(37) $\tau$ PhI(31)
804	2.66	1.36	770	6.20	1.20	762	48.71	0.15	771	772	$\tau$ PhII(29) $\gamma$ CHII(25) $\gamma$ CC(11)
790	3.05	38.68	756	41.23	6.21	740	2.26	45.68	745	-	$\gamma$ CHII(51) $\tau$ PhII(22) $\gamma$ CBr(11)
789	49.46	5.19	755	2.89	39.04	738	77.80	0.91	-	-	$\nu$ PhI(33) $\delta$ PhI(10)
770	57.33	2.30	736	48.57	1.97	723	5.18	2.49	708	-	$\delta$ C=O(36) $\gamma$ CC(13) $\tau$ Ring(12)

732	28.91	49.46	701	24.59	55.43	685	22.07	63.20	-	-	$\delta$ PhI(29) $\delta$ CC(25)
701	13.66	1.53	672	14.54	1.53	669	8.11	0.36	668	-	$\tau$ PhI(28) $\tau$ Ring(14) $\gamma$ CC(17)
679	6.63	6.01	652	6.33	6.91	635	8.78	9.12	638	-	$\delta$ PhII(18) $\nu$ CBr(64)
659	12.52	7.81	636	11.92	8.49	621	10.40	9.21	622	-	$\delta$ Ring(41) $\delta$ PhI(16) $\delta$ PhII(14)
641	65.63	3.54	615	64.98	3.86	598	68.22	5.74	-	-	$\delta$ CO(31) $\delta$ PhI(23) $\delta$ PhII(17)
636	120.00	10.85	607	114.74	11.54	594	112.02	7.58	-	594	$\tau$ CO(62) $\gamma$ CC(10)
573	9.93	2.41	550	10.54	2.94	541	25.80	3.15	555	-	$\tau$ PhII(39) $\gamma$ CC(22)
569	13.08	9.76	546	13.14	10.39	531	14.49	12.33	531	536	$\delta$ Ring(22) $\delta$ PhII(31)
553	0.19	42.77	531	0.39	44.09	522	0.22	50.57	-	-	$\delta$ Ring(42) $\delta$ PhI(27)

548	5.92	1.32	527	5.78	2.83	518	7.34	1.75	-	-	$\gamma$ CO(28) $\delta$ PhI(12) $\delta$ CC(12)
541	11.09	1.44	520	12.48	1.90	514	12.58	1.54	503	500	$\delta$ PhI(36) $\tau$ PhII(22)
511	2.73	1.40	491	2.81	1.34	489	1.95	0.29	-	-	$\delta$ CC(30) $\delta$ CO(17)
507	1.48	0.36	488	0.70	0.38	483	3.14	1.80	480	474	$\tau$ CC(33) $\tau$ PhI(25) $\tau$ Ring(28)
479	10.69	0.09	460	8.90	0.10	448	11.98	0.84	439	-	$\tau$ PhII(54) $\gamma$ CBr(22)
418	1.97	3.29	404	1.82	3.33	400	1.92	2.36	417	405	$\delta$ PhI(43) $\tau$ Ring(33)
4.06	0.42	6.32	389	0.47	6.24	381	0.38	6.91	-	-	$\delta$ CC(30) $\tau$ PhI(22)
367	5.61	0.77	353	5.11	0.87	347	5.66	0.20	-	-	$\delta$ PhI(22) $\gamma$ CC(16) $\tau$ Ring(14)
359	10.52	2.23	344	10.59	2.65	337	12.34	2.97	-	312	$\delta$ CO(25) $\delta$ CBr(12)

309	5.68	11.26	293	5.35	11.11	286	5.11	12.31	-	-	$\delta$ CBr(28)
											$\tau$ PhII(25)
287	0.14	7.29	277	0.11	7.73	267	0.07	2.57	-	-	$\tau$ PhII(29)
											$\gamma$ CBr(16)
269	0.71	1.85	258	0.79	2.13	254	0.92	2.01	-	227	$\delta$ CBr(40)
											$\delta$ C=C(17)
											$\delta$ CC(13)
224	0.30	4.17	216	0.34	3.96	202	1.08	3.53	-	-	$\gamma$ CC(20)
											$\tau$ CC(26)
192	1.43	2.66	184	1.56	2.64	180	1.45	3.07	-	-	$\delta$ CBr(28)
											$\delta$ CC(19)
180	3.06	0.60	175	2.82	0.55	172	3.32	1.30	-	-	$\tau$ Ring(42)
											$\tau$ PhI(24)
											$\tau$ CC(12)
175	1.01	0.23	169	0.92	0.16	164	1.09	0.31	-	-	$\delta$ CBr(17)
											$\delta$ CC(25)
174	0.72	0.84	167	0.84	0.22	158	0.53	0.57	-	-	$\tau$ PhII(24)
											$\gamma$ CBr(40)
121	0.18	0.66	116	0.16	0.68	109	0.13	0.63	-	-	$\delta$ CC(40)
											$\delta$ Ring(13)

107	0.19	2.01	104	0.21	2.14	93	0.26	0.58	-	-	$\tau$ PhI(22) $\gamma$ CC(13) $\tau$ CC(11)
72	2.67	2.08	70	2.41	2.28	68	2.37	1.97	-	-	$\tau$ CO(39) $\tau$ C=C(14) $\tau$ CC(10)
66	0.32	2.09	64	0.38	1.95	60	0.79	0.83	-	-	$\tau$ CO(36) $\tau$ CC(12)
45	0.03	0.12	43	0.03	0.13	41	0.04	0.27	-	-	$\delta$ C=C(33) $\delta$ CC(49)
27	0.04	0.76	26	0.03	0.73	25	0.06	0.35	-	-	$\tau$ Ring(22) $\gamma$ CC(15) $\tau$ PhI(14)
13	0.05	3.55	13	0.04	3.62	6	0.03	2.94	-	-	$\tau$ CC(32), $\tau$ PhI(24)

---

<sup>a</sup> $\nu$ -stretching;  $\delta$ -in-plane deformation;  $\gamma$ -out-of-plane deformation;  $\tau$ -torsion; PhI- tri-substituted phenyl ring; PhII-1,2-substituted phenyl ring; Ring-quinoline ring; In the assignment column the potential energy distributions are given in brackets.

Table 3. Second-order perturbation theory analysis of Fock matrix in NBO basis corresponding to the intra molecular bonds of the title compound

Donor(i)	Type	ED/e	Acceptor(j)	Type	ED/e	E(2) <sup>a</sup>	E(j)-E(i) <sup>b</sup>	F(i,j) <sup>c</sup>
C1-C2	$\sigma$	1.97310	C1-C6	$\sigma^*$	0.01245	1.53	1.25	0.039
-	-	-	C2-C3	$\sigma^*$	0.04904	1.95	1.16	0.043
-	-	-	C2-N15	$\sigma^*$	0.02251	1.44	1.13	0.036
-	-	-	C3-C14	$\sigma^*$	0.02371	3.65	1.17	0.058
-	-	-	N15-C19	$\sigma^*$	0.02000	4.44	1.17	0.064
C2-C3	$\sigma$	1.97032	C1-C2	$\sigma^*$	0.02474	2.26	1.18	0.046
-	-	-	C3-C4	$\sigma^*$	0.02066	2.32	1.20	0.047
-	-	-	C3-C14	$\sigma^*$	0.02371	2.01	1.17	0.043
C5-C10	$\sigma$	1.97008	C1-C6	$\sigma^*$	0.01245	2.71	1.25	0.052
-	-	-	C3-C4	$\sigma^*$	0.02066	3.96	1.20	0.062
-	-	-	C4-C5	$\sigma^*$	0.01952	1.23	1.23	0.035
-	-	-	C5-C6	$\sigma^*$	0.02470	1.37	1.18	0.036
C10-O11	$\sigma$	1.99271	C5-C6	$\sigma^*$	0.02470	2.18	1.54	0.052
-	-	-	C5-C10	$\sigma^*$	0.06179	1.33	1.45	0.040
C10-O12	$\sigma$	1.96367	C4-C5	$\sigma^*$	0.01952	3.15	1.35	0.059
-	-	-	C10-O12	$\sigma^*$	0.11896	2.41	1.06	0.046
C17-C19	$\sigma$	1.97811	C14-C17	$\sigma^*$	0.01106	1.88	1.25	0.043
-	-	-	C19-C20	$\sigma^*$	0.02746	1.80	1.15	0.041
C19-C20	$\sigma$	1.96834	C2-N15	$\sigma^*$	0.02251	5.46	1.11	0.070
-	-	-	C14-C17	$\sigma^*$	0.01106	2.73	1.22	0.052
-	-	-	N15-C19	$\sigma^*$	0.02000	1.14	1.14	0.032
-	-	-	C17-C19	$\sigma^*$	0.04102	1.32	1.13	0.035
-	-	-	C20-C22	$\sigma^*$	0.01430	2.13	1.26	0.046
-	-	-	C22-C24	$\sigma^*$	0.02443	5.25	1.11	0.068
C24-C26	$\sigma$	1.97671	C22-C24	$\sigma^*$	0.02443	3.04	1.17	0.053
-	-	-	C24-C25	$\sigma^*$	0.02320	2.25	1.22	0.047
-	-	-	C26-C29	$\sigma^*$	0.02358	2.24	1.24	0.047
C26-C29	$\sigma$	1.98029	C22-C24	$\sigma^*$	0.02443	4.78	1.18	0.067

-	-	-	C24-C26	$\sigma^*$	0.04050	2.43	1.23	0.049
LP O11	$\sigma$	1.97615	C5-C10	$\sigma^*$	0.06179	3.53	1.10	0.056
-	-	-	C10-O12	$\sigma^*$	0.11896	1.54	0.95	0.035
LP O11	$\pi$	1.86239	C5-C10	$\sigma^*$	0.06179	15.71	0.68	0.094
-	-	-	C10-O12	$\sigma^*$	0.11896	32.30	0.53	0.117
LP O12	$\sigma$	1.97983	C10-O11	$\sigma^*$	0.01909	6.14	1.09	0.073
LP O12	$\pi$	1.83339	C10-O11	$\pi^*$	0.26701	42.27	0.31	0.105
LP O12	$n$	1.52361	C5-C10	$\sigma^*$	0.06179	3.97	0.98	0.063
-	-	-	C10-O11	$\sigma^*$	0.01909	1.21	1.07	0.037
-	-	-	C10-O12	$\sigma^*$	0.11896	7.62	0.83	0.078
LP N15	$\sigma$	1.92430	C1-C2	$\sigma^*$	0.02474	1.46	0.83	0.031
-	-	-	C2-C3	$\sigma^*$	0.04904	11.73	0.81	0.088
-	-	-	C17-C19	$\sigma^*$	0.04102	11.80	0.80	0.087
-	-	-	C19-C20	$\sigma^*$	0.02746	1.79	0.78	0.034
LP Br34	$\sigma$	1.99049	C24-C26	$\sigma^*$	0.04050	1.99	1.19	0.044
LP Br34	$\pi$	1.97168	C24-C26	$\sigma^*$	0.04050	3.41	0.79	0.046
-	-	-	C26-C29	$\sigma^*$	0.02358	2.57	0.81	0.041
LP Br34	$n$	1.93812	C24-C26	$\sigma^*$	0.04050	8.33	0.30	0.049

<sup>a</sup>E(2) means energy of hyperconjugative interactions (stabilization energy).

<sup>b</sup>Energy difference between donor and acceptor i and j NBO orbitals.

<sup>c</sup>F(i,j) is the Fock matrix element between i and j NBO orbitals.

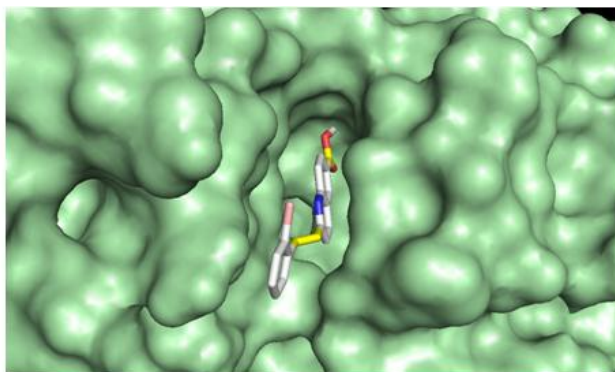
Table4. Experimental and calculated  $^1\text{H}$  NMR parameters (with respect to TMS).

Protons	$\sigma_{\text{TMS}}$	B3LYP/SDD	$\delta_{\text{calc}} = \sigma_{\text{TMS}} - \sigma_{\text{calc}}$	Exp. ( $\delta_{\text{ppm}}$ )
7 H	32.7711	24.0981	8.67	8.26
8 H	-	23.7963	8.97	8.10
9 H	-	22.7194	8.05	8.10
13 H	-	28.0325	8.74	8.67
16 H	-	24.4972	8.27	8.00
18 H	-	24.5939	8.18	8.63
21 H	-	23.0929	7.68	7.57
23 H	-	25.1226	7.65	7.57
28 H	-	25.2309	7.54	7.34
31 H	-	25.1166	7.65	7.50
32 H	-	24.7367	8.03	7.95
33 H	-	25.0668	7.70	7.74

---

## Graphical abstract

Title of the paper: Molecular structure, FT-IR, FT-Raman, NBO, HOMO and LUMO, MEP, NLO and molecular docking study of 2-[(*E*)-2-(2-bromophenyl)ethenyl]quinoline-6-carboxylic acid



## Highlights

- \* IR, Raman spectra and NBO analysis were reported.
- \* The wavenumbers are calculated theoretically using Gaussian09 software.
- \* The geometrical parameters are in agreement with that of similar derivatives.
- \* Molecular docking is reported.

ACCEPTED MANUSCRIPT